Accepted Manuscript

A new age model for the middle Eocene deep-marine Ainsa Basin, Spanish Pyrenees

J.I. Scotchman, P. Bown, K.T. Pickering, M. BouDagher-Fadel, N.J. Bayliss, S.A. Robinson

PII: S0012-8252(14)00204-9
DOI: doi: 10.1016/j.earscirev.2014.11.006
Reference: EARTH 2055

To appear in: *Earth Science Reviews*

Received date: 15 March 2014
Accepted date: 12 November 2014

Please cite this article as: Scotchman, J.I., Bown, P., Pickering, K.T., BouDagher-Fadel, M., Bayliss, N.J., Robinson, S.A., A new age model for the middle Eocene deep-marine Ainsa Basin, Spanish Pyrenees, *Earth Science Reviews* (2014), doi: 10.1016/j.earscirev.2014.11.006

A new age model for the middle Eocene deep-marine Ainsa Basin, Spanish Pyrenees

J.I. Scotchman[1,2]*, P. Bown[1], K.T. Pickering[1], M. BouDagher-Fadel[1],N.J. Bayliss[1,3], & S.A. Robinson[1,4]

[1]Department of Earth Sciences, University College London (UCL), Gower Street, WC1E 6BT, UK

[2]Neftex Petroleum Consultants, 97 Jubilee Avenue, Abingdon, OX14 4RY, UK

[3]ExxonMobil Production Company, Houston, Texas, USA

[4]Department of Earth Sciences, University of Oxford, South Parks Road, Oxford, OX1 3AN, UK

*Corresponding author: j.scotchman@ucl.ac.uk

Abstract: The middle Eocene Ainsa Basin, Spanish Pyrenees, comprises ~4 km of deep-marine sedimentary rocks belonging to the Hecho Group. Despite extensive study of these exemplary deep-marine clastic successions, there has been no comprehensive chronostratigraphic framework that provides primary ages for the submarine fan and related deposits. Here, we present a new composite basin stratigraphy based upon biostratigraphic analyses of the Upper Hecho Group submarine-fan and interfan deposits. Calcareous nannofossil data suggest that deposition of the Gerbe through to Guaso systems occurred during biozones NP14-16 (42.6 and 48.9 Ma based on our age model). Additional biostratigraphic ages from the Lower Hecho Group suggest that the entire Hecho Group no older than biozone NP13 (~51 Ma). The improved chronostratigraphic control enables correlations between submarine canyons and submarine-fans of the Ainsa and Jaca basins to be assessed. Our new age model provides a means of comparison of stratigraphic events with regional sections allowing a better understanding of the lateral and temporal evolution of these depositional systems from source-to-sink.

Supplementary material: Sample location details, examples of larger benthic foraminiferal tests, age calculations and palaeontological results.

Keywords: Ainsa Basin, Hecho Group, turbidites, biostratigraphy, nannofossil, larger benthic foraminifera, Eocene

1.0 Introduction

The Hecho Group deposits of the Ainsa Basin, south central Pyrenees, provide an ideal natural laboratory for the study of the syn-tectonic evolution of siliciclastic submarine-fan and related systems. The easily accessible, 3-D exposures have been used as hydrocarbon-reservoir analogues, resulting in these outcrops being the focus of considerable research, many academic and industrial field-based courses, and numerous research publications (Mutti, 1983; Mutti *et al*. 1985; Remacha *et al*. 2003; Pickering and Bayliss, 2009; Falivene et al. 2010; Moody *et al*. 2012; Dakin *et al*. 2013; Cantalejo and Pickering, 2014; Heard *et al*. 2014). Despite this large body of work, there has been no comprehensive chronostratigraphic framework for the entire Ainsa Basin based on direct sampling of the submarine-fan and related deposits. Reasons for this lack of comprehensive chronostratigraphic framework are due to the commonly poor preservation and/or paucity of calcareous nannofossil and planktonic foraminifera within the Ainsa and Jaca basins (Payros *et al*. 1999; Payros *et al*. 2009).

Existing stratigraphic ages are largely based on correlations with shallow-marine successions around the basin margins (Kapellos and Schaub, 1973; Bentham and Burbank, 1996; Payros *et al*. 2009; Mochales *et al*. 2012a) or correlations with adjacent basins, especially the Jaca Basin to the west (Labaume *et al*. 1985; Payros *et al*. 1999; Oms *et al*. 2003). The value of these studies, however, is dependant upon the reliability of intra- and inter-basin correlations and is problematic because of the absence of Hecho Group deposits in the Boltaña

Anticline zone that separates the Ainsa and Jaca basins (*cf*. Das Gupta and Pickering, 2008; Caja *et al*. 2010). Existing primary ages based upon direct sampling of the Ainsa Basin sediments are of low resolution and restricted to a short stratigraphic interval, within the Ainsa System (Jones *et al*. 2005; Pickering and Corregidor, 2005).

The lack of a robust age model for the Ainsa Basin successions means that critical questions regarding the rate, pacing and underlying control of deep-marine submarine fans and related deposits remain unanswered. In this paper, we seek to address this important problem by presenting new calcareous nannofossil and larger benthic foraminifera data collected from transects through the Upper Hecho Group in the Ainsa Basin. Our study provides the first systematic direct dating of the Ainsa Basin succession and permits the testing of lateral correlations with the adjacent Jaca and Tremp-Graus basins. Such biostratigraphic control is essential when attempting to link these local depositional systems to regional and global events.

1.1 Study area – the Ainsa Basin

1.1.1 Basin development

The middle Eocene Ainsa Basin is a NNW-SSE orientated, thrust-top (piggyback) basin in the south-central Spanish Pyrenees (Fig. 1). The basin forms part of the Middle Eocene foreland basin that developed to the south of the rising Pyrenean orogen (Muñoz, 1992). The present eastern and western margins of the basin are defined by the Mediano and Boltaña anticlines, which separate the Ainsa Basin from the Tremp-Graus Basin to the east and the Jaca Basin to the west (Fig. 1). The Cotiella thrust complex (Muñoz *et al*. 1986) marks the northern margin of the basin, whilst the frontal ramp of the Gavarnie nappe (Sierras Marginales thrust) lies to the south. Syn-tectonic deposition within the basin records the upward stratigraphic evolution from lower to middle Eocene (Ypresian-Lutetian) deep-marine sediment gravity-flow deposits (SGFs) of the Hecho Group, to upper middle to upper Eocene prograding fluvio-delatic systems of the

Sobrarbe and Escanilla formations (Bentham *et al*. 1993; Dreyer *et al*. 1999; Pickering and Bayliss, 2009).

The deep-marine parts of the Ainsa Basin initially developed in response to the early Eocene emplacement of the first major Pyrenean thrust sheet (referred to as the 'Upper Thrust Sheet' by Muñoz *et al*. 1986) resulting in the expansion of the South Pyrenean Central Unit and the associated western lateral-ramp zone creating the Mediano Anticline (Muñoz *et al*. 1986; Farrell *et al*. 1987). The development of the Mediano Anticline created a submarine intraslope tectonic structure that effectively pinned the shelf edge during early basin development and later separated the shallow-marine and terrestrial Tremp-Graus Basin from the deep-marine Ainsa and Jaca basins to the west (Holl and Anastasio, 1993). Loading of the lithosphere led to increased flexural subsidence rates within the foreland, thereby creating an east-to-west axial drainage system (Puigdefabregas *et al*. 1992). Within the developing Tremp-Graus and Ainsa-Jaca basins, the first siliciclastic sediments of the coeval Lower-Middle Montanyana and Lower Hecho groups were deposited above the shallow-marine carbonates of the Alveolina Limestone Formation (Puigdefabregas and Souquet, 1986; Nijman, 1998).

The timing of the transformation of the Ainsa Basin to a thrust-top basin remains controversial, but may correspond with the early Lutetian emplacement of the Pyrenean Lower Thrust Sheet (Muñoz *et al*. 1986; Muñoz, 1992). Thrusting propagated along, and was lubricated by, lower Triassic Keuper evaporites below the Tethyan carbonates (Farrell *et al*. 1987; Muñoz, 1992; Teixell, 1996). The Boltaña Anticline is inferred to have acted as a submarine sill that periodically restricted water mass circulation between the Ainsa and more distal Jaca basins leading to periodic low oxygen levels (Heard *et al*. 2008). The growth of the Boltaña Anticline resulted in the deflection of the structural confinement of sediment gravity-flows, including turbidity currents, but did not prevent their continued westward travel into the Jaca Basin (Labaume *et al*. 1985; Farrell *et al*. 1987).

The final stage of basin development (late Eocene-Oligocene) was associated with the continued emplacement of the Gavarnie thrust slice, thereby increasing the aerial extent of the Pyrenean Axial Zone antiformal stack, and eventually leading to the emergence of the Sierre Exteriores during the Oligocene (Puigdefabregas and Souquet, 1986; Puigdefabregas *et al*. 1992; Teixell, 1996). Even with this increased Axial Zone thickening, the Ainsa Basin experienced a decreased rate of subsidence and reduced shortening rates (Verges *et al*. 1995; Bentham and Burbank, 1996; Verges *et al*. 2002), possibly the result of sub-crustal thermal re-equilibrium associated with the collapse of the subducting/underplating continental slab (Puigdefabregas *et al*. 1992), and/or the progressive shift in deformation southwards towards the Ebro Basin. The reduction in subsidence rates, coupled with an increase in sediment supply from the uplifting Axial Zone, led to shallowing of water depths in the foreland basin (Labaume *et al*. 1985; Puigdefabregas *et al*. 1992). Subsequent basin infill included fluvio-deltaic sediments that generated an overall westward-prograding clastic wedge into the Ainsa Basin and, locally, southward into the Jaca Basin (Bentham and Burbank, 1996; Hogan and Burbank, 1996; Dreyer *et al*. 1999).

1.1.2 Ainsa Basin stratigraphy

The many sedimentological and stratigraphic studies of the Ainsa Basin and adjacent areas have given rise to a confusing array of stratigraphic nomenclature, with the deep-marine deposits referred to as either the Hecho Group (Mutti *et al*. 1972) or the San Vicente Formation (Van Lunsen, 1970). Here, we adopt the stratigraphic divisions of Pickering and Bayliss (2009) that are based upon those of Mutti *et al.* (1972), with alternative nomenclature and previous age dating summarised in Figure 2.

The Hecho Group sediments within the Ainsa Basin consist of ~4 km of siliciclastic SGF and hemipelagic deposits that have been stratigraphically subdivided based upon the presence

of unconformities and their correlative conformities (Fig. 2) (Mutti, 1983; Remacha *et al*. 2003; Hoffman *et al*. 2009; Pickering and Bayliss, 2009). Division of the Hecho Group into Upper (Banaston, Ainsa, Morillo and Guaso systems) and Lower (Fosado, Los Molinos, Arro and Gerbe systems) stratigraphic units is principally based upon the differential tectonic deformation (folding and thrusting) observed within both units. The Lower Hecho Group deposits are typically more intensely folded, sheared and thrusted when compared with the Upper Hecho Group (Pickering and Bayliss, 2009). The contrasting deformation between the two "subgroups" has been linked with the emplacement of the so-called Lower Thrust Sheets (Larra-Boltaña thrust sheet) during the latest Ypresian, interpreted as marking the transition from a foreland basin, *sensu stricto*, to a thrust-top basin (Remacha *et al*. 2003; Pickering and Bayliss, 2009). Here, we suggest that the Upper and Lower Hecho Group boundary should be placed at the base of the Gerbe System rather than at the base of the Banaston System for reasons outlined below.

The Hecho Group can be further subdivided into eight depositional systems (Fosado, Los Molinos, Arro, Gerbe, Banaston, Ainsa, Morillo and Guaso) based upon the identification of lateral shifts in the depositional axes of coarse clastic deposition within the basin, and is speculatively interpreted as the result of tectonic interplay between the Mediano and Boltaña anticlines (*cf*. 'see-saw' tectonics of Pickering and Bayliss, 2009). The stacking of the sandbodies (submarine fans) within these eight systems shows an overall westward/south-westward migration through time away from the deformation front, although the inception of each succeeding system shows the depositional axis relocating back towards the east/north-east. The Morillo and Guaso systems, however, show greater vertical aggradational stacking, interpreted as a response to the tightening of the Mediano (including Añisclo) and Boltaña anticlines (Pickering and Bayliss, 2009). Each of the eight depositional systems, and their component sandbodies, are interpreted as representing the proximal parts of topographically- and structurally-confined, coarse-grained and sand-rich, lower-slope / proximal basin-floor

submarine-fans and associated interfan marlstones (Pickering and Bayliss, 2009). Two to six discrete sandbodies/fans are contained within each system, which comprise a sand-prone interval (interpreted as channelised deposits) and a marlstone-rich interval (interpreted as fan abandonment, fan lateral-margin or interfan sediments). In total, there are 22 to 25 sandbodies, each ~30 to 100 m thick (Pickering and Bayliss, 2009). We refer to these sandbodies as fans, with the inter-sandbody (mappable) marlstone intervals referred to as interfan sediments. In the axial part of the Ainsa Basin, each submarine fan tends to contain a basal chaotic deposit of a sediment slide, slump or pebbly mudstone (debrites), or a combination of all three. These basal chaotic deposits are referred to as mass transport complexes or 'MTCs' with individual depositional events termed mass transport deposits or 'MTDs' (Pickering and Corregidor, 2005). These basal MTCs are typically overlain by a predominantly sandy interval of sediment gravity flow deposits, some of which show an overall thinning-and-fining-upward trend. Thus, the youngest sediments in these successions tend to be much finer grained, and have been interpreted as fan abandonment deposits that pass upwards into interfan marlstones. The development of this idealised vertical sequence was divided into a four-stage process-model (Pickering and Bayliss, 2009), and interpreted initially as resulting from tectonic processes (Pickering and Corregidor, 2005), but later revised to incorporate climatic drivers (Pickering and Bayliss, 2009; Cantalejo and Pickering, 2014). Biostratigraphic age control is essential in order to determine which of these driving mechanisms controlled submarine-fan deposition.

Stratigraphic correlations of the Hecho Group between the Ainsa and Jaca basins remain controversial, due to the lack of preserved sediments on the Boltaña Anticline and the absence of direct dating of the Ainsa Basin submarine-fan systems. Using sandstone petrography, two contrasting correlations between the Ainsa and Jaca depositional systems have been proposed (Das Gupta and Pickering, 2008; Caja *et al*. 2010). Temporal constraints on Ainsa Basin SGF deposits are largely dependent upon correlations with the down-flow Jaca Basin, which itself has not been systematically dated. With inter-basin correlations remaining uncertain, along with

significant lateral variability and/or discontinuity within these clastic sediments, result in the current temporal uncertainty. Correlations between the Hecho Group and its age-equivalent shallow-marine (mainly deltaic) deposits of the Montanyana Group, immediately east of the Mediano Anticline, are equally problematic due to insufficient dating and lack of detailed lateral correlations between stratigraphic units (Fig. 2) (Mutti, 1983; Mutti *et al*. 1985; Puigdefabregas and Souquet, 1986; Nijman, 1998).

Clearly, direct dating of the individual depositional systems within the Ainsa Basin is essential in order to resolve both the temporal framework of the Ainsa submarine fans and related deposits, and to facilitate better correlations between the deposits of the Ainsa Basin, the region of its sediment supply in the Tremp-Graus basin, and the distal, down-current successions of the Jaca Basin. In this study, we have focussed on the Upper Hecho Group, as the Lower Hecho Group shows considerable structural complexity, with abundant shear surfaces, meso-scale folding and faulting (Farrell *et al*. 1987; Muñoz *et al*. 1994; Poblet *et al*. 1998).

2.0 Material and methods

A composite Ainsa Basin stratigraphy (Fig. 4; Supplementary Table S1) was compiled from mainly off-axis sections, as these are most likely to contain common and predominantly *in-situ* microfossils. The Upper Hecho Group sediment thickness was determined from detailed measured sections (Guaso, Ainsa and Banaston systems), recovered core (e.g., Wells A6, L1 and L2) and published studies. Where direct thickness measurements were not available they were estimated from the Ainsa Basin geological map compiled by Pickering and Bayliss (2009), and converted to stratigraphic thickness using measured dips (Fig. 3). Thickness estimates were calculated in this manner for the Morillo System and the Upper Hecho Group stratigraphy below the top of the Banaston-III submarine fan sandstones. Axial sediments were used in the

lower Banaston System, as this is where the majority of palaeontological samples were collected. The lower and upper limits of the measured stratigraphy are pinned at the base of the Gerbe System (Pickering and Bayliss, 2009) and top of the Sobrarbe Formation (Mochales *et al*. 2012a), respectively.

Micropalaeontological samples were collected along selected transects throughout the basin (Fig. 3; Supplementary Table S2) and where possible, both larger benthic foraminiferal (LBF) and hemipelagic sediment samples (for nannofossil analysis) were collected from the same stratigraphic position. LBF samples were collected as individual tests, taken directly from outcrop, or as LBF-rich sediment samples. When LBF samples were taken from sandstone SGF deposits, hemipelagic sediments were collected from stratigraphically adjacent horizons, as these are more likely to contain common and *in situ* planktonic fossils.

Samples were located within the basin stratigraphy using GPS locations and/or known positions within the measured sections. When collected away from measured sections, the samples were located based upon their position relative to laterally extensive deposits, usually submarine fans. Where marker horizons are used for correlation they were assumed to be isochronous.

Calcareous nannofossils were analysed using simple smear slides and standard light microscope techniques (Bown and Young, 1998). Data was collected semi-quantitatively using a Zeiss Axiophot photomicroscope at x 1,000 magnification. Abundance and preservation categories are given in Supplementary Table S4. Biostratigraphy is described with reference to the Paleogene NP zones of Martini (1971) and age calibrations for individual biohorizons are sourced from Gradstein *et al.* (2012)/Time Scale Creator 6.1, unless stated otherwise. The term ‘first occurrence’ (FO) is used for the first or stratigraphically lowest occurrence of the species in the section and is assumed to approximate the evolutionary appearance of the species, unless stated otherwise. The term ‘last occurrence’ (LO) is used for the last or stratigraphically highest occurrence of the species in the section and is assumed to approximate the extinction of the

species, unless stated otherwise.

LBF samples requiring disaggregation were initially fragmented using a hammer and placed in boiling water for ~1 hour and subsequently passed through a very-fine sieve to remove clay- and silt-sized particles. Samples were placed within crucibles and dried overnight at ~50˚C. Liberated tests were hand picked from the sediment and the residue set aside. Thin sections were created using randomly selected tests from each sample or directly from bulk sediment samples. LBF biostratigraphy is described with reference to the SBZ zones of Serra-Kiel *et al.* (1998) and age calibrations for individual biohorizons are sourced from Gradstein *et al.* (2012)/Time Scale Creator 6.1, unless stated otherwise.

The Upper Hecho Group age model was constructed using the NP nannofossil zone marker events as these represent discrete data points relative to the lower resolution LBF or shallow benthic zones (SBZ). Additional nannofossil biohorizons were also included, as discussed below. In all cases we have principally applied nannofossil biohorizons that have published age calibrations. The upper and lower boundaries of each SBZ were positioned midpoint between adjacent sample points representing contrasting assemblages. Nannofossil event positions represent midpoints between samples containing the first (FO) or last (LO) occurrence of a specific species and adjacent samples including or excluding that species. The gradients and intercepts determined from the nannofossil event midpoints were used to estimate the age for each system and its constituent sandy submarine fans plus interfan deposits. Sediment accumulation rates (SAR) were determined between selected nannofossil bioevents and, where necessary, extrapolated to encompass the entire Upper Hecho Group.

3.0 Results

A composite stratigraphy for the Upper Hecho Group was constructed around the measured sections marked in Figure 3. The total stratigraphic section in the Upper Hecho Group

measures vertically 2,134 m, from the base of the Gerbe System to the top of Sobrarbe Formation. Individual system, submarine-fan and associated interfan marlstone thickness estimates are provided in Supplementary Table S1.

Nannofossil biostratigraphic range data are presented for 67 samples (Tables 1, S4). All samples contain nannofossils but in some intervals (Fosado, Arro and Gerbe systems) they are rare. This rarity most likely reflects dilution of the pelagic signal by clastic sedimentary particles. The Guaso, Morillo, Ainsa and Banaston systems samples contain relatively common nannofossils that are moderate and well preserved. Species richness is variable, but the richest assemblages comprise around 50 species. All assemblages are dominated by species of *Coccolithus* and reticulofenestrids (*Reticulofenestra* and *Cyclicargolithus*), and, in general, the zonal marker species are very rare. Reworked Cretaceous nannofossils are consistently present in the samples, but are typically subordinate in abundance to the Eocene taxa.

The nannofossiliferous samples range in age from Zone NP14 in the Gerbe System to Zone NP16 at the top of the Guaso System. The age diagnostic biohorizons are listed in Table 1, with well-established zonal marker taxa in bold, however, all the taxa listed have relatively restricted stratigraphic ranges. The Lower Hecho Group Fosado, Arro and Charo samples contain no definitive zonal marker species, but the presence of *Reticulofenestra* spp., *Discoaster kuepperi*, *Girgisia gammation* and absence of *Lanternithus minutus*, *Pemma* spp., *Blackites inflatus* and *Discoaster sublodoensis* indicates they can be assigned to nannofossil zone NP13 (see for example Agnini *et al*. 2006). Images of individual nannofossil marker taxa are shown in Figure 5.

The LBF assemblages from 35 samples are in general well preserved and common, and contain age diagnostic species throughout the Upper Hecho Group (Table 1). High concentrations are commonly associated with MTCs/MTDs and sandstone SGF deposits. The marker species identified within the Upper Hecho Group indicate the presence of LBF zones SBZ13 to 17 (Serra-Kiel *et al*. 1998). It was not possible to differentiate zones SBZ15 and 16.

When samples contain larger benthic foraminifera representative of multiple biozones (e.g., sample M005 contains *N. articus* and *N. perforatus* indicative of zones SBZ16 and 17, respectively) the younger marker species is assumed to represent the maximum depositional age. The full stratigraphic distribution of larger benthic foraminifera and images of selected LBF tests are available in Supplementary Table S5.

Using these micropalaeontological results, an age model for the Upper Hecho Group of the Ainsa basin is constructed using nannofossil biohorizon points for the Upper Hecho Group and extrapolated into the Sobrarbe Formation (Fig. 6). We have also included palaeomagnetic age information for the Guaso System-Sobrarbe Formation boundary (top Chron C20n) and top of the Sobrarbe Formation (top Chron C19n) taken from Mochales *et al*. (2012a). Using this age model, the age of the individual systems and submarine fans was calculated (Table 2). The age model suggests the Gerbe – Guaso system sediments accumulated over 6.3 Myr, between 42.6 to 48.9 Ma. Sediment accumulation rates (SAR) for the Upper Hecho Group ranges between 18 and 51 cm/kyr (Fig. 6).

4.0 Discussion

4.1 Reliability of palaeontological data

Age-diagnostic nannofossil taxa are typically rare in the Ainsa basin assemblages so, whilst most of these biohorizons have reasonably well constrained age calibrations, there will be some uncertainty in identification of the precise position of first or last occurrences due to the low specimen counts. Furthermore, within these dynamic depositional systems the probability of reworking microfossils is high, and, while reworked fossils of distinctly different ages are easy to distinguish, it is much more difficult if microfossils of similar age are mixed. Despite nannofossil analyses indicating the presence of reworked Cretaceous taxa, the youngest taxa present (those of middle Eocene age) are most likely *in situ* and, therefore, can be considered reliable

age indicators. Reworking most obviously affects the use of last occurrence biohorizons, as it may extend the stratigraphic range of the marker taxon up-section, and so give erroneously old ages. However, in these sediments, with rare and sporadic occurrences of marker species, the first occurrence of a rare taxon could also represent reworked specimens and similarly provide an erroneously old age. However, despite these caveats, the *in situ* middle Eocene nannofossil assemblages are stratigraphically coherent and the bioevents occur in the predicted order, and so we consider that they most likely represent the depositional age of the sediments. The presence of Cretaceous nannofossil taxa is supportive of the Upper Hecho Group sediments including a component of eroded Mesozoic carbonate sediments from the Tremp-Graus Basin (Weltje *et al*. 1996; Das Gupta and Pickering, 2008; Caja *et al*. 2010).

Although we have included the FO of *Reticulofenestra umbilicus* in our age model, large reticulofenestrids (>14µm), which are difficult to accommodate within existing species concepts, start to appear within the Ainsa System succession, prior to the first occurrence of specimens that we unequivocally identify as *R. umbilicus* (see examples in Fig. 5). This calls into question the reliability of this biohorizon. It is notable that the reticulofenestrid coccoliths, in general, are rather diverse but difficult to classify within existing taxonomic schemes, and these middle Eocene representatives require further work before their biostratigraphic significance can be confidently established.

The concentration of LBF within MTC/MTD and sandstone deposits is clear evidence of transportation and re-deposition of these fossils into the deeper-marine Ainsa Basin from shallow-marine habitats, such as those existing in the nearby and coeval Tremp-Graus Basin and basin margin highs (Nijman and Nio, 1975). Although the LBF specimens are allogenic, their delivery and deposition was likely to have been essentially instantaneous, during storm and slope failure processes. However, reworking may have occurred within the shallow marine Tremp-Graus Basin prior to deposition in the Ainsa Basin, resulting in the mixing of LBF species of different ages. Despite this, the LBF marker species occur in expected stratigraphic order and

broadly agree with the nannofossil bioevents (Fig. 6) and, therefore, are here considered biostratigraphically reliable.

4.2 Comparison with previous age estimates from the Ainsa Basin

Existing chronostratigraphic control on the pacing of submarine fan accumulation within the Ainsa Basin is sparse, with published data limited to the Ainsa System (Jones *et al*. 2005; Pickering and Corregidor, 2005). Herein we estimate that the Ainsa System accumulated between 43.7 to 46.0 Ma, which broadly corresponds to the ~43 Ma mid-Lutetian (planktonic foraminifera P11-P12 boundary) and broader Lutetian ages previously proposed (Jones *et al*. 2005; Pickering and Corregidor, 2005).

The cessation of deep-marine deposition within the Ainsa Basin has been suggested to have occurred between 41.6 to 42.3 Ma, based upon LBFs (Zone SBZ15) in the basal deltaic sediments of the Sobrarbe Formation and palaeomagnetic data identified as the top of chron C20n (Bentham and Burbank, 1996; Dreyer *et al*. 1999; Mochales *et al*. 2012a). In our age model, the top of the Upper Hecho Group corresponds to a dark shale horizon located at the top of the Guaso System (sample MFS-4), referred to as the 'anoxic level' by Mochales *et al.* (2012a). Using magnetostratigraphy, Mochales *et al.* (2012a) date this horizon as 42.4 Ma (recalculated to GTS2012), which is consistent with the 42.6 Ma determined for our age model, above the FO of *R. umbilicus* (Table 2; upper dashed line in Fig. 6).

Palaeomagnetic dating of the San Vicente Formation (Paules and Patra members; Mochales *et al.* 2012a) from the southern and western margin of the Ainsa Basin indicates an age range between 48.8 and 42.4 Ma. These members represent the lateral equivalent and depositional feather-edge of the Hecho Group deep-marine deposits (Fig. 2) but the ages are consistent with the age model proposed herein.

Other age estimates for the Ainsa Basin submarine fans are inferred from their correlation with erosional (canyons or truncation) surfaces along the eastern edge of the basin. The age of the Fosado System, representing the earliest submarine-fan system, is based upon its SGF deposits onlapping the erosional base of the "Atiart Canyon" (Mutti *et al*. 1985; Muñoz *et al*. 1994). Holl and Anastasio (1993) place the Atiart Canyon (their angular unconformity '3') within chron 22r. Payros *et al*. (2009) further constrain the age of this submarine canyon by using stratal relationships and the dating of correlative sediments within the Campo area. Their age dating is based upon the Atiart Canyon cutting into the Castigaleu Formation, which contains LBF belonging to Zone SBZ10 (Schaub, 1981). The base of the Atiart Canyon is onlapped by Fosado System SGF deposits, which are in turn overlain by distal sediments of the Castissent Formation, which are assigned to LBF *N. praelaevigalus* Zone (SBZ11), nannofossil *D. lodoensis* Zone (NP13) and chrons C23n.2n to C22r in the Campo area (Marzo *et al*. 1988; Serra-Kiel *et al*. 1994; Bentham and Burbank, 1996). Together these data suggest an age for the Fosado System as being no older than chron C23r.1r (~51 Ma) and no younger than Zone SBZ11 and chron C22r (~49 Ma). This age range is consistent with our study indicating that the Fosado System is no younger than biozone NP13. With this temporal control it is possible to confirm the link between the Atiart Canyon and the onlapping Fosado System SGF deposits as suggested by Nijman (1998).

The erosional surface of the "Charo-Lascorz Canyon" represents an incision surface marking the top of the Castissent Group (Mutti *et al*. 1985; Arbués *et al*. 2011; Muñoz *et al*. 2013). Subsequent deposition within the canyon consists of turbidite deposits assigned the CS2 and Santa Liestra stratigraphic intervals that are correlated with the Gerbe System (Mutti *et al*. 1985; Arbués *et al*. 2011; Muñoz *et al*. 2013). Chronostratigraphic control on the age of the Charo-Lascorz Canyon is provided by Holl and Anastasio (1993) who place the erosive surface (their erosional surface '2') within chron C21n. Dating of the canyon infill is provided by Payros *et al.* (2009) who suggest the basal CS2 turbidites of Millington and Clark (1995) accumulated

during subzone NP15a. Integrating these chronostratigraphic constraints with our dating of the Gerbe System, here dated as accumulating during zone NP14, suggest the following; the Charro-Lascorz Canyon was incised during zones NP14 and chron C21n based upon the correlation between the Gerbe System SGF deposits and the Charo-Lascorz Canyon; backfilling of the proximal canyon in the Charo area continued through to subzone NP15a.

Using an alternative model, an additional intra-Castissent Group erosive surface is identified within the Charo area thereby suggesting a two-phase development of the Charo Canyon (Mutti *et al*. 1985; Millington and Clark, 1995). This intra-Castissent Group canyon is correlated with the Arro System within the Ainsa Basin (Mutti *et al*. 1985; Millington and Clark, 1995). Based upon the magnetostratigraphic dating of the Atiart and Charo-Lascorz canyons, this intra-Castissent Group unconformity formed between chrons C22n and C21n (Holl and Anastasio, 1993). Biostratigraphic dating of the Arro System SGF deposits suggest deposition occurred during biozone NP13 based upon the occurrence of *C. floridanus* within sample AB012 (upper Arro System SGF deposits). The overlying Charo Canyon is onlapped within the Ainsa Basin by the Gerbe System SGF deposits belonging to biozone NP14. Based upon these chronostratigraphic constraints, and the dating of the underlying earlier Atiart Canyon, it is possible to suggest that this intra-Castissent group unconformity developed during NP13 and was filled by biozone NP14. It remains uncertain whether the Charo Canyon developed in a single (Mutti *et al*. 1985) or multple phases (Muñoz *et al*. 1998; Payros *et al*. 2009; Arbués *et al*. 2011; Muñoz *et al*. 2013).

Currently within the literature at least three models exist linking the “Formigales Canyon” to different horizons within the deep-water stratigraphy of the Ainsa Basin. The model of Mutti *et al.* (1985) links the Formigales Canyon with the base of the Banaston System SGF deposits. The alternative model of Arbues *et al*. (2011) suggests the Formigales Canyon separates the Guaso-I and Guaso-II SGF deposits (their O’ Grau and Guaso turbidite systems). A third model places the Formigales Canyon separating the Ainsa and Banaston systems (Barnolas *et al*.

1991). Discerning which of these models is more realistic can be achieved using available chronostratigraphic constraints provided by the data from this paper and previous publications. The Formigales Canyon cuts underlying delta-front deposits of the Capella Formation, which has been assigned to chrons C21n to C20n and European Mammalian Zone MP13 (Cuevas-Gozalo, 1989; Bentham and Burbank, 1996). Therefore the incision of the canyon cannot be older than European Mammalian Zone MP13. Within the Ainsa Basin, temporally equivalent sediments are represented by the Ainsa, Morillo and Guaso systems that are here dated as belonging to biozones NP15-16 (Fig. 6). The base of the older Banaston System is here assigned to biozone NP14 that is older than biozone MP13, resulting in the proposed correlation of Mutti *et al*. (1985) to be discounted. The remaining two correlations linking the Formigales Canyon to the base of the Ainsa or Guaso systems remain both plausible based upon the information provided here. Additional chronostratigraphic constrains upon the age of the sediments infilling the canyon will be required before these two remaining correlations can be adequately tested.

4.3 Position of Lower to Upper Hecho group division

Our age model for the Ainsa Basin Upper Hecho Group suggests that sedimentation was likely relatively continuous throughout the interval. The absence of a lengthy depositional hiatus between the Gerbe and Banaston systems is striking, as this boundary has previously been associated with a significant change in tectonic regime, with greater deformation reported in the older systems (Fig. 1). The absence of a hiatus has led us to reappraise this boundary and we suggest that the Upper/Lower Hecho group division might better be placed below the Gerbe System based upon the following evidence: (1) no discernible hiatus exists between the Gerbe and Banaston systems; (2) the Gerbe System contains abundant pebbly mudstones and pebbly sandstones, in common with the overlying Banaston, Ainsa and Morillo systems, but unlike the

older systems where pebbles are rare and small; (3) the older systems (Fosado – Arro) show meso-scale folding, shearing and thrusting, resulting in vertical to slightly overturned bedding locally (within the Rio Nata valley southwest of Arro village) whilst the younger systems (Gerbe – Guaso) are relatively undeformed; (4) the formation of the Charo-Lascorz Canyon (correlated with the base of the Gerbe System; Muñoz *et al*. 2013; Arbues *et al*. 2011) is attributed to thrusting associated with the formation of the Boltaña Anticline (Millington and Clark, 1995), and potentially linked to the emplacement of the Lower Thrust Sheets (Farrell *et al*. 1987; Mochales *et al*. 2012b); (5) the base of the Campanúe alluvial fan is contemporaneous with the Charo-Lascorz Canyon (Arbués *et al*. 2011; Muñoz *et al*. 2013), linking the Gerbe System with deposition of the Campanúe fluviatile conglomeratic fan, which is dominated by clasts of Cretaceous and Paleocene carbonate rocks that were exposed during a period of renewed uplift within the Axial zone (Weltje *et al*. 1996). The preservation of boulders within the basal deposits of the Gerbe System SGF deposits may represent this influx of sediment.

Together, this evidence suggests that the change in tectonic regime and, therefore, the boundary between the Lower and Upper Hecho groups, more likely occurred prior to the deposition of the Gerbe System, however, further support will require improved understanding of the timing of thrusting in the Pyrenean axial zone and improved dating of the Lower Hecho Group.

4.4 Inter-basin correlations

4.4.1 Ainsa and Tremp-Graus basin correlation

The new age model (Fig. 7) enables the testing of proposed inter-basinal correlations between the deep-marine Ainsa Basin sediments and the mainly terrestrial megasequences of the Tremp-Graus Basin.

The lowermost correlation studied here is the link suggested between Fosado System SGF deposits and the Atiart Canyon (Mutti *et al*. 1985; Barnolas *et al*. 1991; Muñoz *et al*. 1998; Payros *et al*. 2009; Arbués *et al*. 2011; Muñoz *et al*. 2013). With the Atiart Canyon marking the base of the ULM megasequence of Nijman (1998) it would suggest that the Fosado System is the lateral equivalent of the ULM megasequence. Based upon the chronostratigraphic constraints outlined earlier within this paper, this correlation seems robust.

The overlying Arro System of the Ainsa Basin is correlated by many authors with the Castissent Formation (Barnolas *et al*. 1991; Muñoz *et al*. 1998; Arbués *et al*. 2011; Muñoz *et al*. 2013) that accumulated during biozones SBZ11 and NP13 and chrons C23n.2n to C22r in the Campo area (Marzo *et al*. 1988; Serra-Kiel *et al*. 1994; Bentham and Burbank, 1996). Within this study, the Arro System SGF deposits are assignedto the NP13 biozone thereby supporting the correlation between the Arro System and the Casitssent Formation.

The deposition of the Campanue Conglomerates (base of the Santa Liestra Group) within the Tremp-Graus Basin is shown by many authors to be contemporaneous with the deposition of the Gerbe System SGF deposits (Mutti *et al*. 1985; Muñoz *et al*. 1998; Arbués *et al*. 2011; Muñoz *et al*. 2013). Dating of these two units support this temporal correlation with the Campanue Conglomerates (Bentham and Burbank, 1996) and the SGF deposits of the Gerbe System (this study) belonging to chron C21r and biozone NP14, respectively. This temporal correlation may explain the influx of very coarse-grained material into the Ainsa Basin and preserved at the base of the Gerbe System. Additional support is provided by the correlation of the intra-Campanue erosive surface (Besians Channel) with the up-dip equivalent of the Charo Canyon (Barnolas *et al*. 1991). This erosive surface equates to the upper boundary of the UM-C megasequence of Nijman (1998). These relationships therefore link the Gerbe System SGF deposits with, at least in part, to the UM-D megasequence of Nijman (1998) and the Campanue Conglomerates.

Correlations between the younger SGF deposits of the Ainsa Basin (Banaston, Ainsa, Morillo and Guaso systems) with sediments of the Tremp-Graus Basin are inconsistent between studies and based upon the stratigraphic placement of the Formigales Canyon (Mutti *et al*. 1985; Barnolas *et al*. 1991; Arbués *et al*. 2011). Based upon the previously discussed lack of chronostratigraphic constraint upon the Formigales Canyon-Ainsa Basin correlation, we are only able to suggest that the Ainsa, Morillo and Guaso systems (biozones NP15a-NP16) are the temporal equivalents to the Capella Formation (chrons C21n-C20n).

4.4.2 Ainsa and Jaca basin correlation

With Hecho Group sediments being absent over the Boltaña Anticline due to erosion, differing correlations between the Ainsa and Jaca basin submarine-fan systems have been suggested (Mutti *et al*. 1985; Remacha and Fernandez, 2003; Das Gupta and Pickering, 2008; Caja *et al*. 2010). The Ainsa Basin age model presented here enables correlations with the down-current successions of the Jaca Basin (Fig. 1,7).

Current correlations between the deep-marine (Hecho Group) sediments of the Ainsa and Jaca basins suggest the following: Torla-Fosado, Broto-Arro/Los-Molinos, Cotefable-Gerbe, Banaston-Banaston, Jaca-Ainsa/Morillo. Alternatively, Das Gupta and Pickering (2008) suggest a correlation (Torla-Fosado, Broto-Gerbe, Banaston-Cotefablo, Jaca-Ainsa and Rapitan Deposits-Morillo/Guaso) based upon petrographic analysis. Figures 1 and 7 shows the stratigraphic position of the megaturbidites in the Jaca Basin (Labume *et al*. 1985; Remacha *et al*. 2003; Payros *et al*. 2007). To investigate these correlations further, the SGF deposits of the Jaca Basin require more precise age dating. We tentatively suggest the following Jaca-Ainsa inter-basin SGF system correlations: Figols-Fosado/Los Molinos/Arro, Torla-Gerbe, Broto/Cotefablo-Banaston, Banaston-Ainsa/Morillo/Guaso, Jaca-Sobrarbe and Escanilla formations. With these revised inter-basin correlations proposed here, the existing

chronostratigraphic constraints of Jaca Basin SGF systems fit reasonably well within the Ainsa Basin age model proposed here (Figure 6).

4.5 Basin sediment accumulation rates

The age model suggests that sediment accumulation rates (SAR) within the more axial deposits of the Ainsa Basin, varied between 18 and 51 cm/kyr, with a mean of 30 cm/kyr (Figs. 6, 8). These variations can be tentatively related to the tectonic history of the south Pyrenean foreland.

The basal sediments of the Upper Hecho Group record high SARs (40-51 cm/kyr) and are likely related to the period of renewed basin deformation that transformed the simple foreland basin (containing the Jaca, Ainsa and Tremp-Graus basins) to a compartmentalised thrust-top or piggyback basin. The synchronous emplacement of the Gavarnie thrust sheet and associated thickening of the Axial Zone antiformal stack, led to lithospheric loading characterised by a period of increased subsidence rates (Puigdefabregas and Souquet, 1986; Puigdefabregas et al. 1992). Together, these events led to increased accommodation within the foreland basin and denudation of the hinterland thereby enhancing the volume and calibre of the sediment available for transport and subsequent deposition within in the Ainsa Basin (Weltje et al. 1996). This is also consistent with the high sedimentation rates identified within the contemporaneous UM-A to UM-C megasequences of the Tremp-Graus Basin (Nijman, 1998).

The increased volume of sediment available immediately following this tectonic phase of basin reorganisation is shown by the presence of six submarine fans within the Banaston System, the most in any of the eight depositional systems (Pickering and Bayliss, 2009). The increased calibre (bulk mean grain size) of sediment marking the base of the Upper Hecho Group is also apparent with the B-I, B-II and Gerbe System submarine fans containing large

limestone olistoliths, pebbly conglomerates and very-coarse sandstones, the amount of which decrease in subsequent systems.

Following the initial phase of basin re-organisation, thrust propagation and uplift rates decreased, thereby reducing denudation rates and the volume of very coarse material in the staging areas for supply to the deep-marine Ainsa Basin. This reduction in the supply of coarse material is shown by the decrease in SAR, down to ~22-27 cm/kyr after 45.6 Ma and maintained until the final infill of the basin.

Comparison between our SAR estimates and those from the laterally equivalent San Vicente Formation (Mochales *et al*. 2012a) show a striking contrast in rates (Fig. 8). The basin axis submarine fans of this study show greater rates of sediment accumulation compared to the essentially marginal basin settings studied by Mochales *et al.* (2012a) (Fig. 8). The varying rates of SAR recorded along the western basin margin prior to 45 Ma were likely due to uplift and tightening of the Boltaña Anticline, modulating the amount of subsidence and, hence, accommodation space available on the western flank of the anticline. Post 45 Ma, the two records show similar SARs likely due to both studies sampling from more axial basin sediments.

Basin development and the volume and calibre of sediments available for transport into the Ainsa Basin were likely linked, at least at a basin scale, to tectonic events associated with the evolving Pyrenean orogen. Comparing the SAR derived from our study with subsidence histories of other foreland basins, it appears that the development of the Ainsa Basin followed a similar ‘convex-up’ pattern of subsidence with time (e.g., Xie and Heller, 2009).

5.0 Conclusions

We have constructed a new age model for the Upper Hecho Group deposits in the Ainsa Basin, based upon the first systematic palaeontological (calcareous nannofossil and larger benthic foraminifera) direct dating of the submarine-fan and related systems. The age model indicates

that the Upper Hecho Group (here including the Gerbe through Guaso systems) accumulated over a ~6.3 Myr period spanning 42.6 to 48.9 Ma. Although age dating for the Lower Hecho Group is based on fewer samples, these further indicate that the entire Ainsa Basin Hecho Group accumulated over a period of ~9 Myrs, between ~51 and 42.6 Ma. These ages are consistent with previous estimates based largely on magnetostratigraphic studies from the basin margins (e.g., Mochales *et al*. 2012a).

Utilising this new age model, correlations between Ainsa Basin SGF deposits and submarine canyons found in the eastern basin margin were tested and accordingly revised. Using available chronostratigraphic controls, we correlate the Fosado and Gerbe SGF deposits with the Atiart and Charo-Lascorz canyons, respectively. We also tentatively suggest a correlation between the Ainsa-Morillo-Guaso submarine-fan systems and the Formigales Canyon. Correlations between the Ainsa Basin and down-flow Jaca Basin SGF deposits are also re-assessed. The Fosado, Los Molinos and Arro SGF deposits of the Ainsa Basin are correlated with the Figols SGF deposits of the downdip Jaca Basin. The Gerbe and Banaston systems SGF deposits are tied to the Torla, Broto and Cotefablo systems of the Jaca Basin. The Ainsa, Morillo and Guaso systems are dated as being temporally equivalent to the Banaston System of the Jaca Basin. Finally, the Sobrarbe and Escanilla formations are correlated with the Jaca System of the Jaca Basin.

Average sediment accumulation rates (SAR) for the Upper Hecho Group ranged between 18 and 51 cm/kyr, with an average of 30 cm/kyr, and contrast with lower rates at the western basin margin, suggesing the amount of subsidence, and hence accommodation, was likely modulated by uplift of the Boltaña Anticline. The trend of declining SARs through time is comparable with ‘convex-up’ patterns of subsidence observed in other foreland basins.

Finally, our age model will help constrain any evaluation of the lateral and temporal evolution of the depositional systems both within this basin, and in any transect from source to sink. It will also contribute to an improved understanding of tectonics *versus* climatic, autocyclic

versus allocyclic controls on deposition within these basins, something that is beyond the scope of this paper. Comparable high-resolution age dating of the Tremp-Graus and Jaca basins is required before the correlations proposed here can be fully evaluated.

Acknowledgements

ExxonMobil (J.I.S., K.T.P.) are thanked for their generous financial support for this project. Palaeontological work was supported by grants from the UK Natural Environment Research Council (N.J.B.) and Shell, UK (N.J.B.). S.A.R. was supported by a Royal Society URF. The authors also wish to thank J. Davies for micropalaeontological thin-section preparation; the Spanish Governments Ministry of Agriculture, Food and Environment for allowing the use of SIGPAC aerial images; Geological Society of America for allowing the reproduction of the Ainsa Basin geological map; and support from the other members from the UCL Deep-Water Research group. We thank Cai Puigdefabregas and Aitor Payros for their constructive review of earlier versions of this manuscript.

Declaration of interest

None.

References

Agnini, C., Muttoni, G., Kent, D.V. and Rio, D., 2006. Eocene biostratigraphy and magnetic stratigraphy from Possagno, Italy: The calcareous nannofossil response to climate variability. *Earth and Planetary Science Letters*, **241**(3-4), 815-830.

Arbués, P., Butillé, M., López-Blanco, M., Marzo, M., Muñoz, J.A. and Serra-Kiel, J. 2011. Exploring the relationships between deepwater and shallow-marine deposits in the Ainsa piggy-back basin fill (Eocene South-Pyrenean Foreland Basin). In: C. Arenas, L. Pomar and F. Colombo (editors), *Post-Meeting Field Trips Guidebook*, 28th IAS Meeting. Sociedad Geológica de España, Zaragoza, pp. 199-239.

Barnolas, A., Samsó, J.M., Teixell, A., Tosquella, J. and Zamorano, M. 1991. Guide Book 1, Evolución sedimentaria entre la Cuenca de Graus-Tremp y la Cuenca de Jaca-Pamplona. In: F. Colombo (ed.), *I Congreso del Grupo Español del Terciario*, Vic, Spain, pp. 123.

Bentham, P.A. and Burbank, D.W. 1996. Chronology of Eocene foreland basin evolution along the western margin of the South-Central Pyrenees. In: P.F. Friend and C.J. Dabrio (editors), *Tertiary*

basins of Spain, the stratigraphic record of crustal kinematics. Cambridge University Press, Cambridge, pp. 144-152.

Bentham, P.A., Talling, P.J. and Burbank, D.W. 1993. Braided stream and flood-plain deposition in a rapidly aggrading basin: the Escanilla formation, Spanish Pyrenees. *Geological Society, London, Special Publications*, **75**(1), 177-194.

Bown, P.R. and Young, J.R. 1998. Techniques. In: P.R. Bown (ed.), *Calcareous Nannofossil Biostratigraphy*. Chapman & Hall, London, pp. 16-28.

Caja, M.A., Marfil, R., Garcia, D., Remacha, E., Morad, S., Mansurbeg, H., Amorosi, A., Martínez-Calvo, C. and Lahoz-Beltrá, R. 2010. Provenance of siliciclastic and hybrid turbiditic arenites of the Eocene Hecho Group, Spanish Pyrenees: implications for the tectonic evolution of a foreland basin. *Basin Research*, **22**(2), 157-180.

Cantalejo, B. & Pickering, K.T. 2014. Climate forcing of fine-grained deep-marine systems in an active tectonic setting: Middle Eocene, Ainsa Basin, Spanish Pyrenees. *Palaeogeography, Palaeoclimatology, Palaeoecology*, **410**, 351-371.

Cuevas-Gozalo, M.C. 1989. Sedimentary facies and sequential architecture of tide-influenced alluvial deposits. An example from the middle Eocene Capella Formation, South-Central Pyrenees, Spain. PhD Thesis, University of Utrecht, Utrecht, 152 pp.

Dakin, N., Pickering, K.T., Mohrig, D. and Bayliss, N.J. 2013. Channel-like features created by erosive submarine debris flows: Field evidence from the Middle Eocene Ainsa Basin, Spanish Pyrenees. *Marine and Petroleum Geology*, **41**, 62-71.

Das Gupta, K. and Pickering, K.T. 2008. Petrography and temporal changes in petrofacies of deep-marine Ainsa-Jaca basin sandstone systems, Early and Middle Eocene, Spanish Pyrenees. Sedimentology, **55,** 1083-1114.

Dreyer, T., Corregidor, J., Arbues, P. and Puigdefabregas, C. 1999. Architecture of the tectonically influenced Sobrarbe deltaic complex in the Ainsa Basin, northern Spain. *Sedimentary Geology*, **127**(3-4), 127-169.

Falivene, O., Arbues, P., Ledo, J., Benjumea, B., Muñoz, J.A., Fernandez, O. and Martinez, S. 2010. Synthetic seismic models from outcrop-derived reservoir-scale three-dimensional facies models: The Eocene Ainsa turbidite system (southern Pyrenees). *AAPG Bulletin*, **94**(3), 317-343.

Farrell, S.G., Williams, G.D. and Atkinson, C.D. 1987. Constraints on the age of movement of the Montsech and Cotiella Thrusts, south central Pyrenees, Spain. *Journal of the Geological Society*, **144**(6), 907-914.

Gradstein, F.M., Ogg, J.G. and Schmitz, M. 2012. The Geologic Time Scale 2012. *Elsevier Science & Technology Books*, Amsterdam.

Heard, T.G., Pickering, K.T. and Robinson, S.A. 2008. Milankovitch forcing of bioturbation intensity in deep-marine thin-bedded siliciclastic turbidites. *Earth and Planetary Science Letters*, **272**(1-2), 130-138.

Heard, T.G., Pickering, K.T. & Clark, J.D. 2014. Ichnofabric characterization of a deep-marine clastic system: a subsurface study of the Middle Eocene Ainsa System, Spanish Pyrenees. *Sedimentology*, **61**, 1298–1331.

Hoffman, M., Bouroullec, R., Guzofski, C., Pyles, D., Clark, J., Setiawan, P., Moody, J., Silalahi, H. and Moss-Russell, A. 2009. Tectono-Stratigraphic Analysis of a Deep-Water Growth Basin, Ainsa Basin, Northern Spain. *Search and Discovery*, **30102**, 1-30.

Hogan, P.J. and Burbank, D.W. 1996. Evolution of the Jaca piggyback basin and emergence of the External Sierra, southern Pyrenees In: P.F. Friend and C.J. Dabrio (editors), *Tertiary Basins of Spain: The Stratigraphic Record of Crustal Kinematics*. Cambridge University Press, Cambridge, pp. 153-160.

Holl, J.E. and Anastasio, D.J. 1993. Paleomagnetically derived folding rates, southern Pyrenees, Spain. *Geology*, **21**(3), 271-274.

Jones, R.W., Pickering, K.T., Boudagher-Fadel, M. and Matthews, S. 2005. Preliminary observations on the micropalaeontological characterization of submarine fan/channel sub-environments, Ainsa System, south-central Pyrenees, Spain. In: A.J. Powell and J.B. Riding (editors), *Recent Developments in Applied Biostratigraphy*. The Micropalaeontological Society, London.

Kapellos, C. and Schaub, H., 1973. Zur Korrelation von Biozonierungen mit Grossforaminiferen und Nannoplankton im Palaogen der Pyrenaen. *Eclogae Geologicae Helvetiae*, **66**, 687-737.

Labaume, P., Séguret, M. and Seyve, C. 1985. Evolution of a turbiditic foreland basin and analogy with an accretionary prism: Example of the Eocene South-Pyrenean Basin. *Tectonics*, **4**(7), 661-685.

Larrasoaña, J.C., Gonzalvo, C., Molina, E., Monechi, S., Ortiz, S., Tori, F. and Tosquella, J. 2008. Integrated magnetobiochronology of the Early/Middle Eocene transition at Agost (Spain): Implications for defining the Ypresian/Lutetian boundary stratotype. *Lethaia*, **41**(4), 395-415.

Martini, E., 1971. Standard Tertiary and Quaternary calcareous nannoplankton zonation. In: A. Farinacci (ed.), *Proceedings of the Second Planktonic Conference Roma 1970*. Edizioni Tecnoscienza, Rome, pp. 739-785.

Marzo, M., Nijman, W. and Puigdefabregas, C.A.I. 1988. Architecture of the Castissent fluvial sheet sandstones, Eocene, South Pyrenees, Spain. *Sedimentology*, **35**(5), 719-738.

Millington, J.J. and Clark, J.D. 1995. The Charo/Arro canyon-mouth sheet system, south-central Pyrenees, Spain; a structurally influenced zone of sediment dispersal. *Journal of Sedimentary Research*, **65**(4b), 443-454.

Mochales, T., Barnolas, A., Pueyo, E.L., Serra-Kiel, J., Casas, A.M., Samsó, J.M., Ramajo, J. and Sanjuán, J. 2012a. Chronostratigraphy of the Boltaña anticline and the Ainsa Basin (southern Pyrenees). *Geological Society of America Bulletin*, **125**(3-4).

Mochales, T., Casas, A.M., Pueyo, E.L. and Barnolas, A. 2012b. Rotational velocity for oblique structures (Boltaña anticline, Southern Pyrenees). *Journal of Structural Geology*, **35,** 2-16.

Moody, J.D., Pyles, D.R., Clark, J. and Bouroullec, R. 2012. Quantitative outcrop characterization of an analog to weakly confined submarine channel systems: Morillo 1 member, Ainsa Basin, Spain. *AAPG Bulletin*, **96**(10), 1813-1841.

Muñoz, J.-A., Beamud, E., Fernández, O., Arbués, P., Dinarès-Turell, J. and Poblet, J. 2013. The Ainsa Fold and thrust oblique zone of the central Pyrenees: Kinematics of a curved contractional system from paleomagnetic and structural data. *Tectonics*, **32**(5), 1142-1175.

Muñoz, J.A. 1992. Evolution of a continental collision belt: ECORS-Pyrenees crustal balanced cross-section. In: K.R. McClay (ed.), *Thrust Tectonics*. Chapman and Hall, London, pp. 235-246.

Muñoz, J.A., Arbues, P. and Serra-Kiel, J. 1998. The Ainsa Basin and the Sobrarbe oblique thrust system: sedimentological and tectonic processes controlling slope platform sequences deposited synchronously with a submarine emergent thrust system. In: A. Melendez Hevia and A.R. Soria (editors), *15th International Sedimentological Congress*. International Association of Sedimentologists, Alicante, pp. 213-223.

Muñoz, J.A., Martinez, A. and Vergés, J. 1986. Thrust sequences in the eastern Spanish Pyrenees. *Journal of Structural Geology*, **8**(3-4), 399-405.

Muñoz, J.A., McClay, K.R. and Poblet, J. 1994. Synchronous extension and contraction in frontal thrust sheets of the Spanish Pyrenees. *Geology*, **22**(10), 921-924.

Mutti, E. 1983. The Hecho Eocene Submarine Fan System, South-Central Pyrenees, Spain. *Geo-Marine Letters*, **3**, 199-202.

Mutti, E., Luterbacher, H.P., Ferrer, J. and Rossell, J. 1972. Schema stratigrafico e lineamenti di facies del Paleogene marino della zona centrale sudpirenaica tra Tremp (Catalogna) e Pamplona (Navarra). *Memorie della scoieta geologica italiana*, **11**, 391-416.

Mutti, E., Remacha, E., Sgavetti, M., Rosell, J., Valloni, R. and Zamorano, M. 1985. Stratigraphy and facies characteristics of the Eocene Hecho Group turbidite systems, south-central Pyrenees. In: M.D. Mila and J. Rosell (editors), *6th European Regional Meeting of the International Assocaiation of Sedimentologists*. International Assocaiation of Sedimentologists, Lleida, pp. 521-576.

Nijman, W. 1998. Cyclicity and basin axis shift in a piggyback basin: towards modelling of the Eocene Tremp-Ager Basin, South Pyrenees, Spain. *Geological Society, London, Special Publications*, **134**(1), 135-162.

Nijman, W. and Nio, S.D. 1975. The Eocene Montanana Delta (Tremp-Graus Basin, Provinces Lerida and Huesca, Southern Pyrenees, N. Spain) In: J. Rosell and C. Puigdefabregas (editors), *9th International Sedimentological Congress International Association of Sedimentologists*, Nice.

Oms, O., Dinarès-Turell, J. and Remacha, E. 2003. Magnetic Stratigraphy from Deep Clastic Turbidites: An Example from the Eocene Hecho Group (Southern Pyrenees). *Studia Geophysica et Geodaetica*, **47**(2), 275-288.

Payros, A., Bernaola, G., Orue-Etxebarria, X., DinarÈS-Turell, J., Tosquella, J. and Apellaniz, E. 2007. Reassessment of the Early–Middle Eocene biomagnetochronology based on evidence from the Gorrondatxe section (Basque Country, western Pyrenees). *Lethaia*, **40**(2), 183-195.

Payros, A., Pujalte, V. and Orue-Etxebarria, X. 1999. The South Pyrenean Eocene carbonate megabreccias revisited: new interpretation based on evidence from the Pamplona Basin. *Sedimentary Geology*, **125**(3-4), 165-194.

Payros, A., Tosquella, J., Bernaola, G., Dinarés-Turell, J., Orue-Etxebarria, X. and Pujalte, V. 2009. Filling the North European Early/Middle Eocene (Ypresian/Lutetian) boundary gap: Insights from the Pyrenean continental to deep-marine record. *Palaeogeography, Palaeoclimatology, Palaeoecology*, **280**(3-4), 313-332.

Pickering, K.T. and Bayliss, N.J. 2009. Deconvolving tectono-climatic signals in deep-marine siliciclastics, Eocene Ainsa basin, Spanish Pyrenees: Seesaw tectonics versus eustasy. *Geology*, **37**(3), 203-206.

Pickering, K.T. and Corregidor, J. 2005. Mass-Transport Complexes (MTCs) and Tectonic Control on Basin-Floor Submarine Fans, Middle Eocene, South Spanish Pyrenees. *Journal of Sedimentary Research*, **75**(5), 761-783.

Poblet, J., Muñoz, J.A., Travé, A. and Serra-Kiel, J. 1998. Quantifying the kinematics of detachment folds using three-dimensional geometry: Application to the Mediano anticline (Pyrenees, Spain). *Geological Society of America Bulletin*, **110**(1), 111-125.

Puigdefabregas, C., Muñoz, J.A. and Verges, J. 1992. Thrusting and foreland basin evolution in the Southern Pyrenees. In: K.R. McClay (ed.), *Thrust Tectonics*. Chapman & Hall, London, pp. 247-254.

Puigdefabregas, C. and Souquet, P. 1986. Tecto-sedimentary cycles and depositional sequences of the Mesozoic and Tertiary from the Pyrenees. *Tectonophysics*, **129**(1-4), 173-203.

Remacha, E. and Fernandez, L.P. 2003. High-resolution correlation patterns in the turbidite systems of the Hecho Group (South-Central Pyrenees, Spain). *Marine and Petroleum Geology*, **20**(6-8), 711-726.

Remacha, E., Oms, O., Gual, G., Bolano, F., Climent, F., Fernandez, L.P., Crumeyrolle, P., Pettingill, H., Vicente, J.C., Suarez, J. and Arcuri, M. 2003. *Geological Field Trip 12, South-Central Pyrenees, Spain*, AAPG International Conference and Exhibition. Total, Barcelona, Spain.

Schaub, H. 1981. Nummulites et Assilines de la Tethys paleogene. Taxonomie, phylogenese et biostratigraphie. *Schweizerische Paläontologische Abhandlungen*, 104. Editions Birkhäuser, Bale, 236 pp.

Serra-Kiel, J., Canudo, J.I., Dinarès, J., Molina, E., Ortiz, N., Pascual, J.O., Samso, J.M. and Tosquella, J. 1994. Cronostratigrafia de los sedimentos marinos del Terciario inferior de la Cuenca de Graus-Tremp (Zona Central Surpirenaica). *Revista de la Sociedad Geológica de España*, **7**(3-4), 273-297.

Serra-Kiel, J., Hottinger, L., Caus, E., Drobne, K., Ferrandez, C., Jauhri, A.K., Less, G., Pavlovec, R., Pignatti, J., Samso, J.M., Schaub, H., Sirel, E., Strougo, A., Tambareau, Y., Tosquella, J. and Zakrevskaya, E. 1998. Larger foraminiferal biostratigraphy of the Tethyan Paleocene and Eocene. *Bulletin de la Societe Geologique de France*, **169**(2), 281-299.

Teixell, A. 1996. The Anso transect of the southern Pyrenees: basement and cover thrust geometries. *Journal of the Geological Society*, **153**(2), 301-310.

Van Lunsen, H.A. 1970. Geology of the Ara-Cinca Region, Spanish Pyrenees, Province of Huesca, Utrecht University, 119 pp.

Verges, J., Fernandez, M. and Martinez, A. 2002. The Pyrenean orogen: pre-, syn-, and post-collisional evolution. *Journal of the Virtual Explorer*, **8**, 57-76.

Verges, J., Millán, H., Roca, E., Muñoz, J.A., Marzo, M., Cirés, J., Bezemer, T.D., Zoetemeijer, R. and Cloetingh, S. 1995. Eastern Pyrenees and related foreland basins: pre-, syn- and post-collisional crustal-scale cross-sections. *Marine and Petroleum Geology*, **12**(8), 903-915.

Weltje, G.J., Van Ansenwoude, S.O.K.J. and de Boer, P.L., 1996. High-frequency detrital signals in Eocene fan-delta sandstones of mixed parentage (south-central Pyrenees, Spain); a reconstruction of chemical weathering in transit. *Journal of Sedimentary Research*, **66**(1), 119-131.

Xie, X. and Heller, P.L., 2009. Plate tectonics and basin subsidence history. *Geological Society of America Bulletin*, **121**(1-2), 55-64.

Fig. 1. (**a**) Schematic summary stratigraphy of the Hecho and Montanyana groups within the South Pyrenean foreland Tremp-Graus, Ainsa and Jaca basins. Sediments were supplied axially from alluvial fans within the Tremp-Graus Basin. Within the Ainsa Basin, the accumulation of channelised submarine-fans was mainly confined between the Mediano and Boltaña anticlines. West of the Boltaña Anticline, sediments of the Jaca Basin consist mainly of submarine lobes and related deposits, including basin-wide megaturbidites (MT-1 to MT-8). Erosive canyons identified within the eastern Ainsa Basin margin labelled A (Atiart), C (Charro) and F (Formingales). (**b**) Location of study area (Ainsa Basin) in the south-central Pyrenees, northern Spain.

Fig. 2. Summary of chronostratigraphy and stratigraphic terms used for the Tremp-Graus, Ainsa and Jaca basins. Current dating of the submarine fans within the Ainsa Basin is based upon lateral correlation with the equivalent submarine lobe sediments within the more distal and down-current Jaca Basin. In this study, the Ainsa Basin stratigraphic divisions of Pickering and Bayliss (2009) are used. Timing of the Boltaña and Mediano anticline formation from Remacha *et al*. (2003) and Holl and Anastasio (1993), respectively.

Fig. 3. Sample localities and measured section shown on the Ainsa Basin geological map of Pickering and Bayliss (2009). Palaeontological samples were collected throughout the Upper Hecho Group together with additional locations within the Lower Hecho Group. Details are given within Table S2. Detailed logging and drilling of the Ainsa wells (Pickering and Corregidor, 2005; Pickering and Clark, 2012) provide accurate stratigraphic thickness estimates of several sections. The positions of the wells and logged sections are provided in Supplementary Figure S1. The thickness of other stratigraphic intervals were estimated using distances and dips obtained from the geological map. Samples collected from the Lower Hecho Group and sample MFS-4 are not shown here but their GPS positions are provided in Table S2.

Fig. 4. Composite Upper Hecho Group stratigraphy determined from detailed measured sections and basin geological map. Palaeontological samples collected from throughout the Upper Hecho Group and placed within stratigraphy to enable the construction of an age model (Fig. 6).

Fig. 5. Examples of the age-diagnostic nannofossil taxa used to construct the Hecho Group age model. Calcareous nannofossils were analysed using simple smear slides and standard light microscope techniques (Bown and Young, 1998). Data was collected semi-quantitatively using a Zeiss Axiophot photomicroscope at x 1000 magnification, with a minimum of 1000 fields of view examined for each sample.

Fig. 6. The Upper Hecho Group age model is based upon the composite Upper Hecho Group stratigraphy (Fig. 4) and biostratigraphic events (Table 1) identified in this study. Nannofossil events are used here to construct the age model as these represent discrete points in time rather than board shallow benthic zones (grey boxes). Sediment accumulation rates are determined for each interval. The equations of the lines between the nannofossil biostratigraphic events are used to date the Upper Hecho Group along with the calculation of sediment accumulation rates (Tables S3, S4). Jaca Basin SGF deposits are shown with temporal constraints from the literature and stratigraphic correlation with the Ainsa Basin SGF deposits as proposed in this study.

Fig. 7. Simplified chronostratigraphy of the Hecho and Montanyana group sediments of the Jaca, Ainsa and Tremp-Graus basins based upon the discussion within section 4.4.
The timing of Ainsa Basin submarine-fan systems and related deposits are based upon this study with the age of the Sobrarbe and Escanilla formations additionally constrained by

Mochales *et al*. (2012a). Ages of the Atiart (A), Charo (C) and Formigales (F) submarine canyons are based upon studies outlined in the text. Dating of the Jaca Basin submarine-fan systems are based upon the dating of megaturbidites (MT) (Payros *et al*. 1999; Oms *et al*. 2003; Payros *et al*. 2007). Jaca Basin tectonostratigraphic unit (TSU) divisions from Remacha *et al*. (2003). Solid and dashed horizontal lines represent high and low confidence chronostratigraphic boundaries.

Fig. 8. Sediment accumulation rates for the Ainsa Basin calculated for the basin axis and western margin. Within the basin axis, variations in these accumulation rates may coincide with several distinct phases of tectonic activity within the South Pyrenean Central Unit (refer to discussion). Differing amounts of accommodation space were created upon the western basin margin (Paules and Las Patra members) due to the developing Boltaña Anticline thereby moderating recorded accumulation rates.

Table 1. *Upper Hecho Group palaeontological results*

Height (m)	Sample	SBZ	SB Marker	Other SB datum	SB event age (Ma)	NP	NP Marker event	Other NP datum	NP event age (Ma)
2133.8	BUIL-3,4,5, D007	17	present *N. brongniarti*, *N. perforatus*	present *N. lyelli*					
1950.8	GU015; GUB015	17				16	present *S. furcatolithoides*	present *C. vanheckiae**, ***C. solitus***, ***D. bifax***†, *S. spiniger*	40.50
1707.3	NS-15						FO ***R. umbilicus***		43.32
1674.6	M005	16/17	FO *N. brongniarti*, LO *N. aturicus*	LO *Ass. exponens*					
1662.3	M004; MB004	16/17		LO *D. balatonica*					
1543.4	M002; MB002							LO *B. virgatus*	43.50
1448.6	M012	16/17	FO *N. perforatus*	FO *N. boussaci*					
1442.5	AI021	16		FO *D. balatonica*	41.15 (top SBZ16)				
1403.4	AI013	16	FO *N. aturicus*						
1400.9	AI011 / AI011B	14?	LO *Ass. spira*		42.57 (top SBZ14)				
1392.5	AIB014					15b	LO ***C. gigas***	FO *B. virgatus*	44.12
1377.9	Ainsa-228.4m	14	LO *N. beneharnensis*, *Alv. munieri*						
1174.5	A6/37-3					15b	FO ***C. gigas***		45.49
1093.6	AI002; AIB002	14		LO *Ass. suteri*					
1093.6	NS-07					15b	FO *S. furcatolithoides*		45.00
1012.9	NS-04							FO *C. vanheckiae*	45.89
1009.9	AI028	14		LO *D. cf. pulcra*, FO *Ass. exponens*					
1007.9	AI027; AIB027	14/13	FO *N. beneharnensis*, *Ass. Spira*, *Alv. munieri*	LO *N. obesus*, FO *N. boussaci*, *D. cf. pulcra*, *Ass. suteri*					
984.2	NS-27							present *B. globosus*	44.81
912.5	B005	13	LO *N. laevigatus*	LO *N. syrticus*, *N. lehneri*, *Ass. Abrardi*	43.57 (top SBZ13)				
758.3	Ban-134.5m					15a	FO ***N. fulgens***		46.29
619.3	B013; BB013	13				14b	LO ***B. inflatus***		46.29‡
589.3	B014	13		FO *N. syrticus*, present *Alv. ellptica*					
471.3	B016; BB016	13		present *N. messinae*, FO *N. lehneri*		14b	FO ***B. inflatus***	present ***D. sublodoensis***§	47.84
402.3	B022	13		FO *N. obesus*					
370.3	B026	13	present *N. laevigatus*	FO *Ass. abrardi*					
104.5	GB001					14	FO *B. piriformis*	LO *G. gammation*, FO *Pemma*, *L. minutus*¶	47.94
-	AB012					?13	FO *C. floridanus*		

*Presence of *C. vanheckiae* plotted as NP16 midpoint (41.64 Ma).
†Presence of *C. solitus* and *D. bifax* plotted as 40.40 Ma.
‡Dating of LO *B. inflatus* from Larrasoaña *et al.* (2008).
§LO of *D. sublodoensis* 47.66 Ma. Here we use age mid-point between LO and FO.
¶Other taxa ~48 Ma.

Table 2. *Calculated stratigraphic unit age and sediment accumulation rate*

Stratigraphic unit	Top age (Ma)*
Sobrarbe Formation	41.66 (41.09)
Guaso-II marlstone	42.55 (42.42)
Guaso-II fan	42.85 (42.77)
Guaso-I marlstone	42.86 (42.78)
Guaso-I sand	43.14 (43.10)
Morillo-III marlstone	43.23 (43.21)
Morillo-III sand	43.36
Morillo-II marlstone	43.45
Morillo-II sand	43.66
Morillo-I marlstone	43.84
Morillo-I sand	44.14
Ainsa-III marlstone	44.24
Ainsa-III sand	45.12
Ainsa-II marlstone	45.38
Ainsa-II sand	45.59
Ainsa-I marlstone	45.64
Ainsa-I sand	45.80
Banaston-VI marlstone	45.82
Banaston-VI sand	45.91
Banaston-V marlstone	45.99
Banaston-V sand	46.26
Banaston-IV marlstone	46.29
Banaston-IV sand	46.54
Banaston-III marlstone	46.59
Banaston-III sand	46.75
Banaston-II sand	46.97
Banaston-I sand	47.56
Gerbe marlstone	48.31‡
Gerbe-I & II sand	48.51‡
Base	48.87‡

*Age estimates calculated from interval equations (Supplementary Table S3). Values in brackets calculated when incorperating the magnetostratigraphic points of Mochales *et al.* (2012a) into the age model.

Fig 1

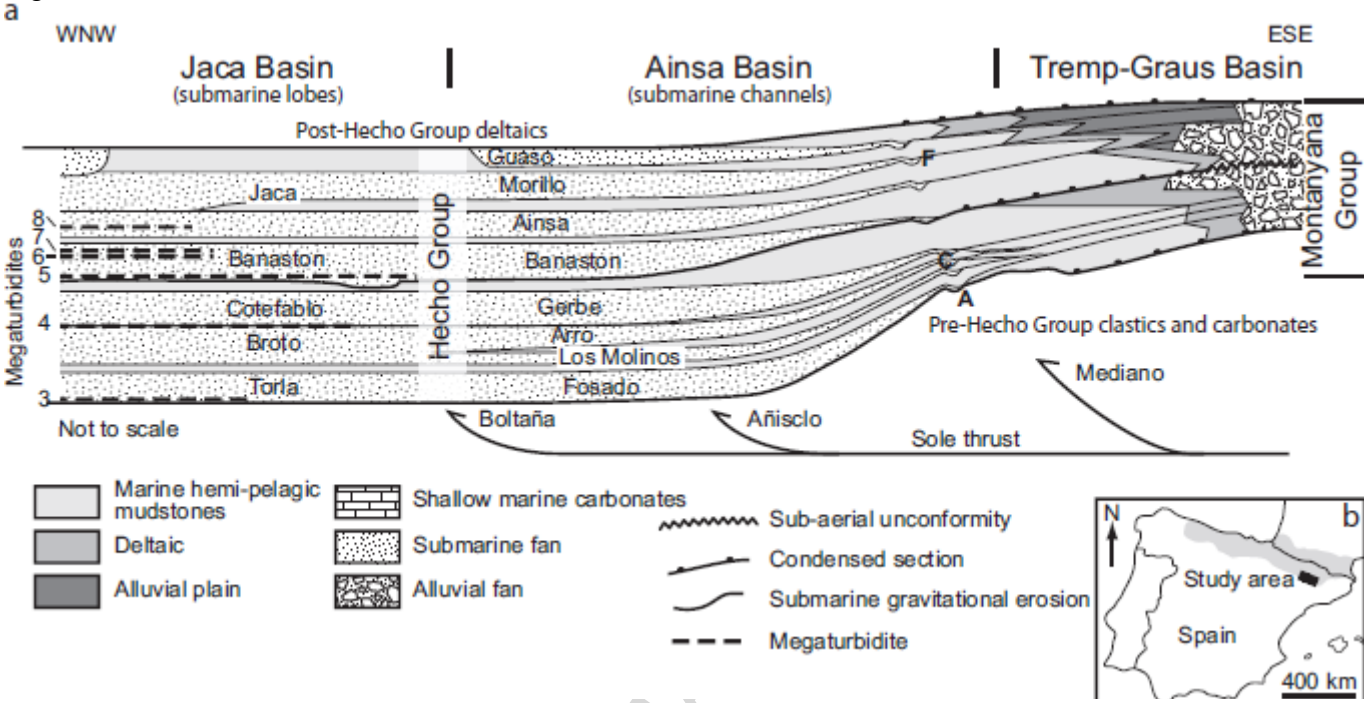

Fig 2

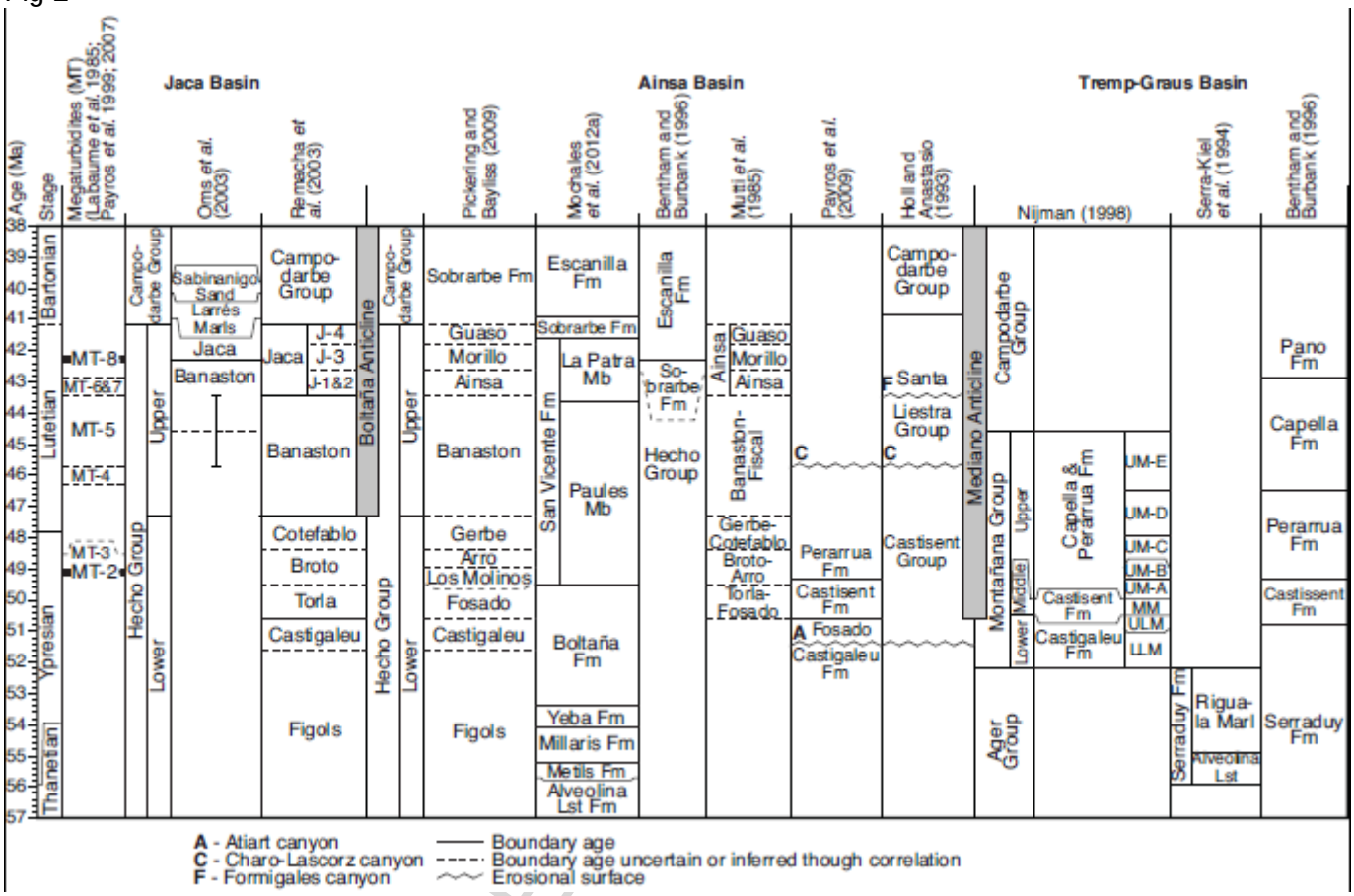

Fig 3

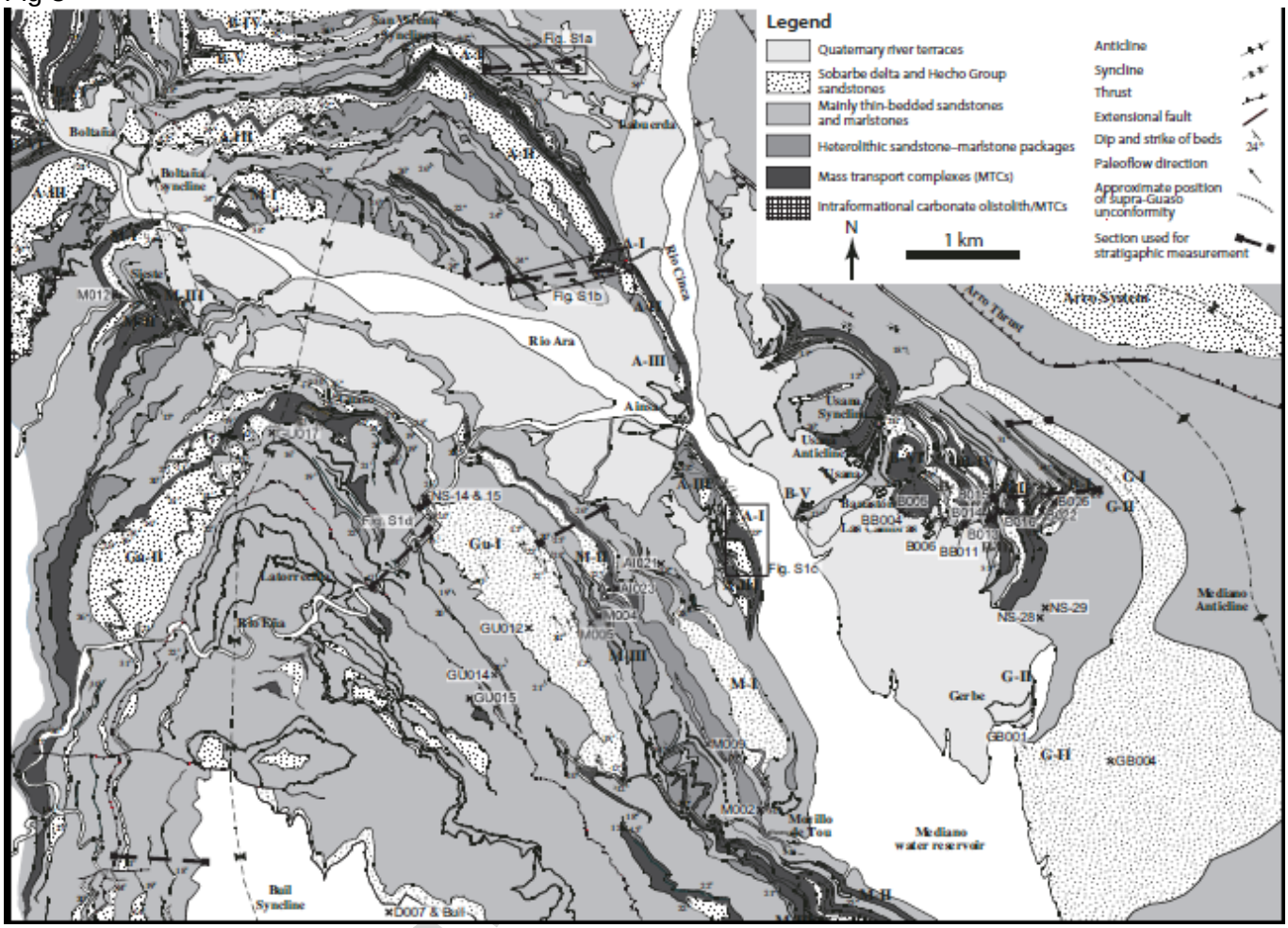

Figure 4

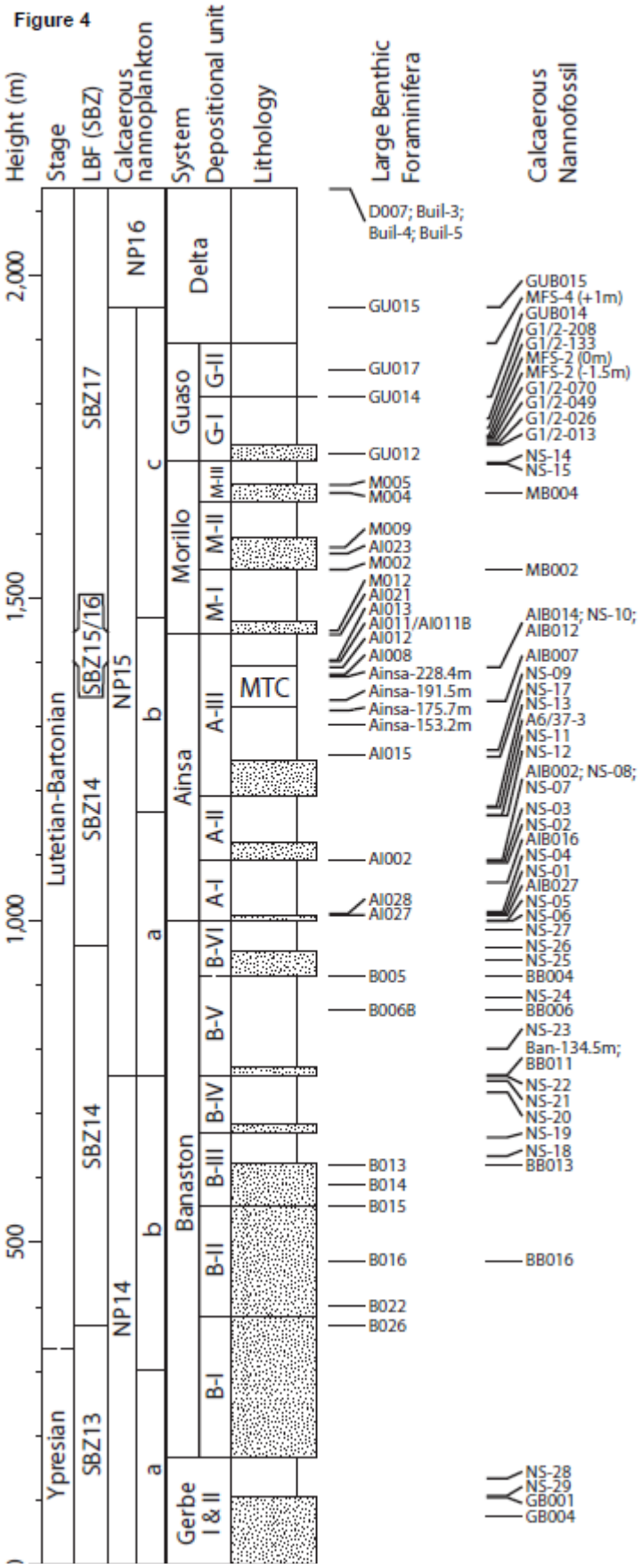

Fig 5

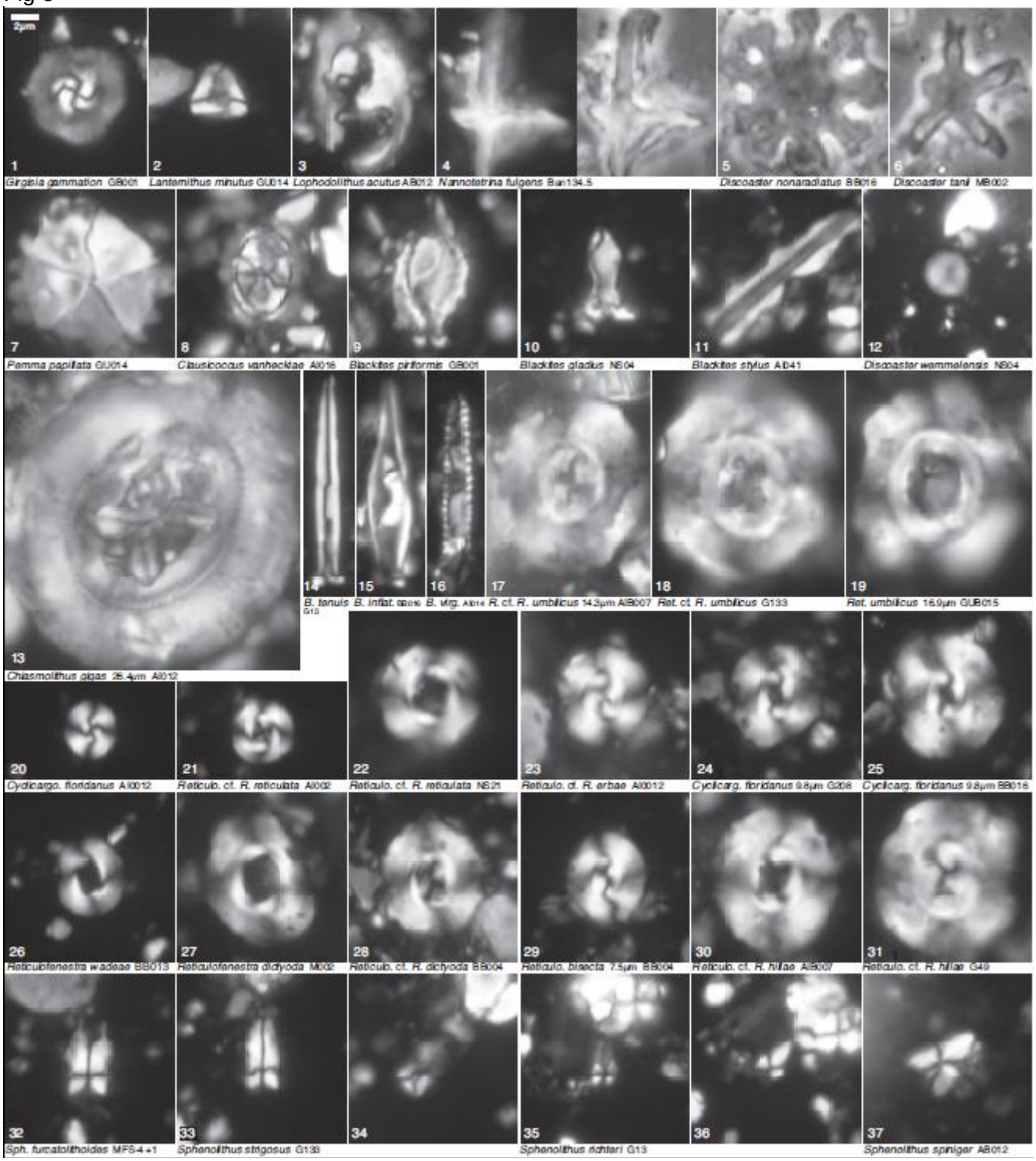

Figure 6

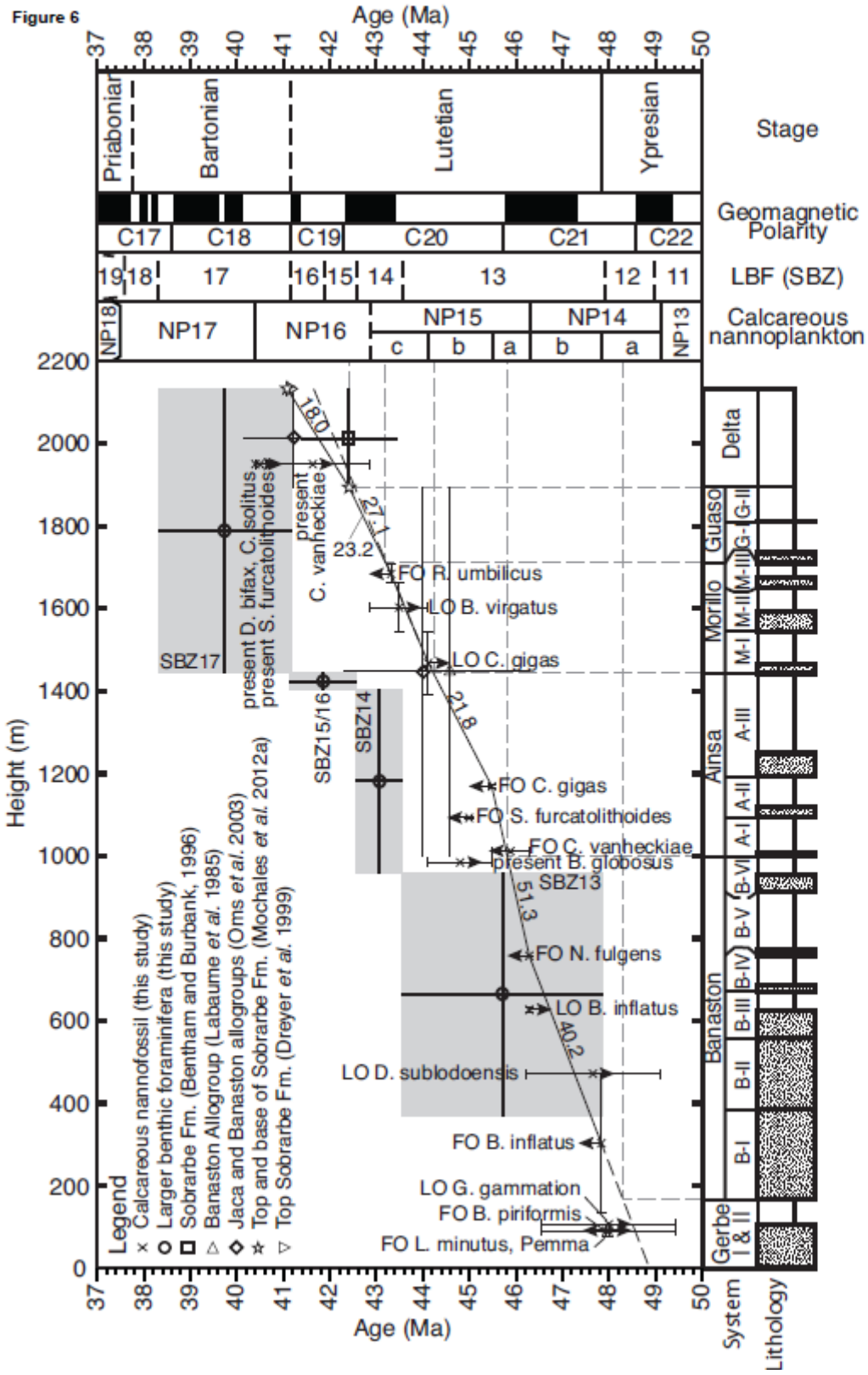

Fig 7

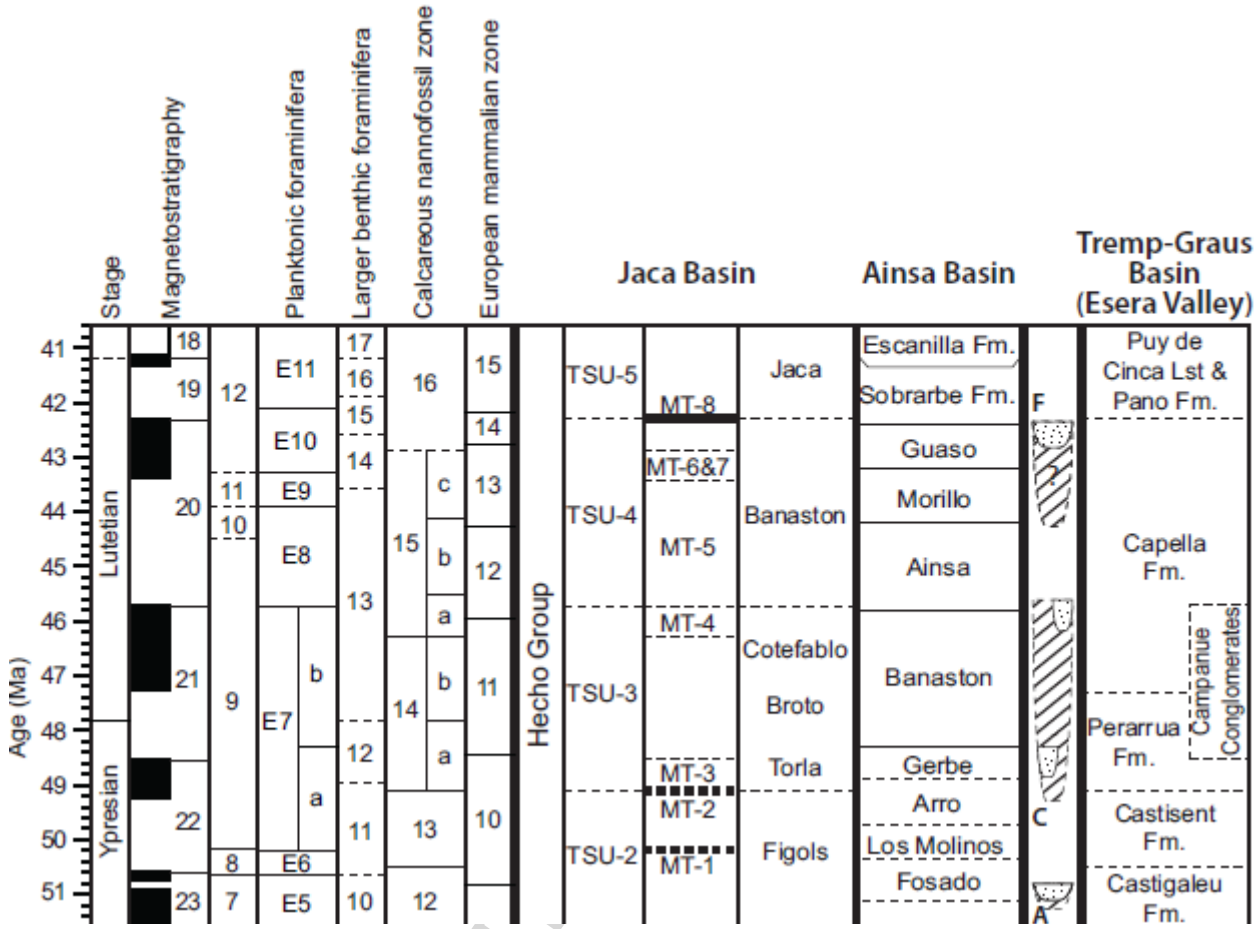

Fig 8